Advanced Journal of Engineering and Scientific Applications (AJESA)

Research Paper Open Access

Available online at www.ajesa.com.ng Vol.1, No.1, 2024. pp.1-15

Effects of Graphene Nanoplatelets at low filler content on tensile and fracture toughness properties of f-GNP/epoxy Nanocomposites

George O. Okoronkwo[1], Nwadike Ethelbert C.[2], Chukwudi Prince E. U.[3]

[1]Department of Chemical Engineering, Micheal Okpara University of Agriculture, Umudike, Abia State, Nigeria;
okoronkwo.george@mouau.edu.ng, ogeorgeonyeka@gmail.com

[2]Department of Civil Engineering, Federal Polytechnic Nekede, Owerri, Imo State, Nigeria;
cnwadike@fpno.edu.ng

[3]Chukwudi Prince E. U., Department of Civil Engineering, Federal Polytechnic Nekede, Owerri, Imo State, Nigeria;
cugonna@fpno.edu.ng

Corresponding Author::ogeorgeonyeka@gmail.com

Abstract

This paper aims at effects of graphene nanoplatelets at low filler content on tensile and fracture toughness properties of plasma functionalized graphene nanoplatelets f-GNP/epoxy nanocomposites. Various mechanical tests were performed on a series of f-GNP/epoxy at low nanofiller loading to assess the effect of the nanofiller on mechanical properties. Most importantly, a significant enhancement in fracture toughness is achieved without compromising the tensile and thermal properties of the nanocomposites. The fracture toughness of neat epoxy resin was increased by over 50 % with the incorporation of 0.25 wt% f-GNP loading, obtaining a value of 245 , while the neat epoxy indicated a value of 162 . The glass transition temperature and coefficient of thermal expansion (CTE) both showed a slight increase of 3 % and 2 %, respectively, both at 1 wt. % f-GNP loading. These enhancements are competitive with current literature results on nanocomposites, but at significantly lower filler content. We therefore demonstrated that f-GNPs are capable of providing effective toughening of epoxy resins, while maintaining other tensile and thermal properties.

KEYWORDS: Epoxy, Nanofiller, Nanocomposite, Strength properties, Fracture toughness

1. INTRODUCTION

The use of two-dimensional (2D) carbon allotropes for reinforcing composite materials has been the focus of extensive research within the field of materials science in recent years. (Boland et al. 2016) Graphene nanoplatelets (GNPs) are regarded as short stacks of less than 10 graphene layers, and may be purchased at a relatively low cost. (Kausar, et al. 2016) GNPs are widely used as nanoadditives for advanced composites, (Sainsbury, et al. 2016) electrodes in advanced batteries and ultra/super capacitors, (Stevens, et al. 2016) and the conductive component in specialty coatings or adhesives. (Zagho et al. 2018) GNPs are also used for exceptionally strong and impermeable packaging, better lubricants, (Tabandeh-Khorshid, et al. 2016) and for highly sensitive strain sensors. (Boland, et al. 2016) The ability to improve the strength and fracture toughness of epoxy with the addition of GNPs at low loading content is a route undertaken by many researchers to face the engineering challenges of producing strong, lightweight materials (Liu, et al. 2016), (Sainsbury, et al. 2016) .

Epoxy resins are widely used for many engineering applications, from composite wind turbine blades in the renewable energy sector to the highly complex structural parts for aircraft. 20–22 Developed in 1960s, the diglycidyl ether of

bisphenol A (DGEBA) resin system is the most commonly used epoxy. (Darshan et al. 2021) Epoxy resins are also extensively employed as engineering adhesives and matrices for fiber-reinforced plastics (FRP) due to their highly beneficial properties such as high adhesion strength and good processability. By reacting the epoxy resin with a suitable curative, three-dimensional cross-linked thermoset structures are obtained, (Darshan et al. 2022) which results in a material with excellent mechanical and thermal properties,26–28 including high modulus, high failure strength, and improved interfacial bonding for many industrial applications. (Darshan et al. 2022) Despite the numerous advantages of epoxy such as excellent mechanical properties and thermal stability, epoxies are fundamentally brittle due to their high cross-link density. (Dornbusch, et al. 2016) Low fracture toughness is one of the key drawbacks preventing the increased use of epoxies for a wider range of applications, and consequently toughening of epoxy resins has been at the forefront of many research studies since the early 1980s. (Namdev et al. 2022) A common approach to increasing the toughness is the addition of a second-phase filler to the matrix at the micro- or nanoscale, resulting in composite materials which exhibit high specific strength and stiffness, and high fracture toughness.2 The key objective of reinforcing epoxies is to allow the desired properties to be tailored according to the engineering needs while keeping the cost low.

(Vinod et al. 2018) studied the effect of the mechanical properties of graphene platelet, single-walled carbon nanotube, and multi-walled carbon nanotube-based epoxy nanocomposites at 0.1 wt% loading. Mode I fracture toughness of the nanocomposite with graphene platelets showed ~53% increase compared to pristine epoxy. (Namdev et al. 2023) studied the effect of SWCNTs, DWCNTs, and MWCNTs on the mechanical properties and the benefits of surface functionalization of CNTs. The pristine epoxy had a mode I fracture toughness was increased by 45% using non-functionalized SWCNT. Increasing the percentage weight content of SWCNT over 0.3% showed a decrease in mode I fracture toughness. They explained the reason for this finding by associating it with re-agglomeration.

The toughening mechanisms of nanosilca-modified epoxy polymers were studied by 39 Silica nanoparticles were incorporated into the epoxy resin via a sol–gel technique. At 13 wt% loading, they observed a significant increment in fracture toughness from 100 to 460 J m−2 which was attributed to the plastic void growth mechanisms as validated by the theoretical model. Glass transition temperature was found to be unchanged by the addition of the nanofiller. Further studies carried out by (Namdev et al. 2020) on hybrid materials that had been formed using an epoxy polymeric matrix and a range of inorganic particles, including mica and organically-modified montmorillonites (organoclays) were also reported. Fracture toughness of the hybrid materials was increased with increasing loading content of the silicate before decreasing at higher loading contents. The toughening mechanisms effect was associated due to plastic deformation of the epoxy matrix.

The amalgamation of rubber along with other potential nanofillers dispersed in epoxy resins (Mushtaq, et al. 2016) (Kumar et al. 2020) has also been an area of interest for many researchers. It was observed that there is a substantial increase in fracture toughness and ductility but also resulted in a decrease in the stiffness and the ultimate tensile strength of the cured polymers. (Li, et al. 2016) Low modulus rubber particles usually decrease the stiffness and thermal properties of polymer- based materials. (Mushtaq, et al. 2016) The work of (King, et al. 2016) focused on the mechanical properties and toughening mechanisms of epoxy using polysiloxane-based core–shell (S–CSR) particles. It was found that the tensile properties of the resulting nanocomposite decreased while a significant improvement in fracture toughness was observed from 117 to 947 after the introduction of S–CSR into the epoxy resin. This effect was attributed to the cavitation of the particles which was followed by void growth.

For effective reinforcement, it is critical to achieve good stress-transfer from the matrix to the filler particles. In order to improve the interfacial bonding, the surface of GNPs has been chemically-modified by several groups. Covalent functionalization of GNPs has been shown to give significant enhancement over non-functionalized platelets in epoxy-nanocomposites. (Backes, et al. 2016) The fracture toughness has been improved by up to 40% over non-functionalized GNPs by covalent functionalization with 4, 4′-diaminophenylsulfone. This was accompanied with a 55 % increase in modulus. (Kemp, et al. 2016) In contrast, similar fracture toughness improvements were seen by using 4, 4′-methylene diphenyl diisocyanate, with no significant improvement in modulus.48

In this paper, a series of low loading (<1 wt%) plasma functionalized-GNP–epoxy nanocomposites were prepared and various properties were investigated to assess the mechanical and thermal properties of the nanocomposites. Impressive Mode I fracture toughness was attained without degrading the strength, stiffness, glass transition temperature or coefficient of thermal expansion (CTE) at low loadings. A thorough method of processing f-GNP into the matrix was adopted, thereby maximizing the dispersion of the nanofiller into the matrix to achieve optimum performance.

2. MATERIALS AND METHODS

2.1 Materials

The resin used in this study was a two-part low viscosity epoxy, Araldite® LY 564 resin, and cycloaliphatic polyamine Aradur® 2954 hardener supplied by Sunday chemicals.. The normal ratio of resin to hardener was 100:35 by weight, with a gel time of approximately 90 min at 60 °C. Graphene nanoplatelets, were provided by Haydale Ltd., which had undergone a proprietary plasma process (HDPlasregistered GNP-O_2-STD, Batch Number: 8039). They were used without further modification. The HDPlas® process is based on a low temperature plasma process which avoids acid treatments on the nanomaterials. Functionalization via plasma enables a more homogenous dispersion to be achieved within the host matrix by introducing the compatible chemical groups to the filler material.

2.2 Characterization methods

Scanning Electron Microscopy (SEM) images were acquired using a ZEISS Supra at an accelerating voltage of 5 kV and a nominal working distance of 2.5 mm. The fracture surface of the nanocomposites specimens were coated in a thin layer of gold (3 nm) in order to enhance contrast due to the latter being non-conductive. X-ray diffraction (XRD) measurements were conducted using a Siemens D5000 diffractometer in conjunction with a Cu–Kα X-ray tube (40 kV, 40 mA) filtered using a Ni filter and anti-scatter and divergences slits of 1 mm under standard θ–2θ conditions. Raman spectra were recorded using a Renishaw inVia Raman Microscope at λ = 514.5 nm and a total laser power incident on the sample of 1 mW. X-ray Photoelectron Spectroscopy (XPS) was performed using a Kratos Axis Ultra DLD system using an Al monochromated X-ray source operated at 15 kV, 5 mA emission. Analysis conditions used were 160 eV pass energy, 1 eV steps, 0.2 s dwell per step, and 2 sweeps. Samples for XPS were prepared by evaporation of GNP from solution onto Si-wafer substrates.

2.3 Compounding of f-GNP/epoxy nanocomposites

All of the nanocomposites in this study were prepared under identical conditions. The required f-GNP loading content was sonicated using a Branson 2510EMT sonic bath, in methanol for 1 h to ensure complete removal of f-GNP aggregates, enabling effective dispersion. To achieve an optimum dispersion of the f-GNPs within the epoxy resin, the f-GNPs were first dispersed within a solvent medium (methanol), which ensured the efficient de-agglomeration of f-GNP stacks by disrupting the van der Waals attractive forces between the nanomaterials. By using an excess of the solvent, the f-GNPs were dispersed in a large solvent volume to which the epoxy resin was added drop wise, stirring continuously. Alternative solvents such as N-methyl-2-pyrolidone (NMP) or dimethylformamide (DMF) are known to provide more readily prepared f-GNP dispersions. However, when considering the final mechanical embodiment of these nanocomposites, it was of the utmost importance to remove all traces of solvent residue which may compromise the strength of the nanocomposites. Hence, in this study, methanol, was chosen as a low boiling point solvent to facilitate the dispersion of the f-GNPs, while allowing its efficient removal. A magnetic stirrer was used to mix the f-GNP/methanol dispersion while the epoxy was added dropwise. A rotorvap operating at 45 °C (10 mbar) was used to evaporate the methanol from the f-GNP–epoxy suspension. The resulting mixture was left in the oven at 45 °C for several days under vacuum at 1 mbar to ensure complete evaporation of methanol. A high speed mixer (Speed Mixer DAC150 FVZ-K, Synergy Devices, UK) operating at 3500 rpm for 12 min was then employed to mix the f-GNP/epoxy nanocomposite. The mixtures were left to stand for several days to allow un-exfoliated flakes to sediment, and the supernatant removed. This will result in a small, systematic, correction to the concentration of f-GNPs in the final composites. The values reported here are therefore nominal concentrations. The neat epoxy underwent identical processing conditions as the f-GNP loadings during the processing stage. Aradur® 2954 hardener was then added to the nanocomposite, which was mixed again using a high speed mixer at 3500 rpm for 45 s. The suspension was further degassed for approximately 45 min and was then poured into an open aluminum dogbone shaped mould, casting specimens for mechanical and thermal testing. Specimens were cured for 1 h at 80 °C followed by 160 °C for 4 h. Samples were prepared with f-GNP loadings between 0.1 and 1 wt% in addition to a control sample of pure epoxy.

2.4 Testing procedure

Tensile testing procedure Uniaxial tensile tests on nanocomposites were performed on the cast dog-bone specimens (see Figure 1) according to ASTM D638 (Type I geometry) using an Instron® universal test machine fitted with a 20 kN load cell. The crosshead speed was set at 2 mm/min and all tests were performed at room temperature. A clip-on extensometer with a 2.5 mm stroke was employed to measure the elongation during the test up to failure point. For each loading content six specimens were tested for statistical evaluation. The Young's modulus (E), ultimate tensile strength (UTS), elongation at break (EL), and toughness (T) (the area under the stress–strain curve of the nanocomposites) were evaluated at the specific filler loadings.

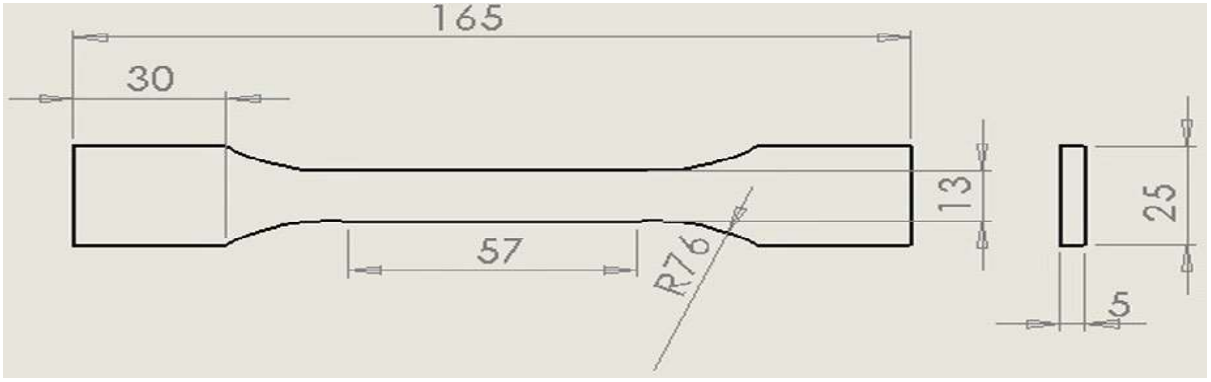

Figure 1. TYPE I tensile test specimen dimensions. Dimensions are in millimeters

2.5 Single-edge-notch bending procedure

In addition to the tensile toughness described above, the fracture toughness of the resulting nanocomposites was investigated according to ASTM D5045 in three-point-bending using single-edge-notch bending (SENB) specimens as shown in Figure 3. A pre-crack of length 2 mm was introduced at the moulded V-notch by tapping a fresh razor blade. Tests were undertaken using an Instron® test machine fitted with a 20 kN load cell at a crosshead speed of 10 mm/min. Six specimens were tested at each nanofiller loading content. The critical stress intensity factor, *KIC*, and the mode I fracture toughness, *GIC*, were calculated according to Equations (1) and (2), respectively.

$$K_{IC} = \frac{F \times L}{B \times W^{\frac{3}{2}}} . f\left(\frac{a}{W}\right) 0 < \left(\frac{a}{W}\right) < 1 \quad (1)$$

where

$$f\left(\frac{a}{W}\right) = 3\left(\frac{a}{W}\right)^{\frac{1}{2}} \left\{ \frac{\left[1.99 - \frac{a}{W}\left(1 - \frac{a}{W}\right)\left(2.15 - 3.93\left(\frac{a}{W}\right) + 2.7\left(\frac{a}{W}\right)^2\right)\right]}{2\left(1 + 2\frac{a}{W}\right)\left(1 - \frac{a}{W}\right)^{\frac{3}{2}}} \right\} \quad (2)$$

and

$$G_{IC} = \frac{1 - \nu^2}{E} . K_{IC}^2 \quad (3)$$

The definitions for the symbols used in the equations are summarized in Table 1. A value of 0.35 was used for Poisson's ratio, as specified on the material supplier's data sheet.

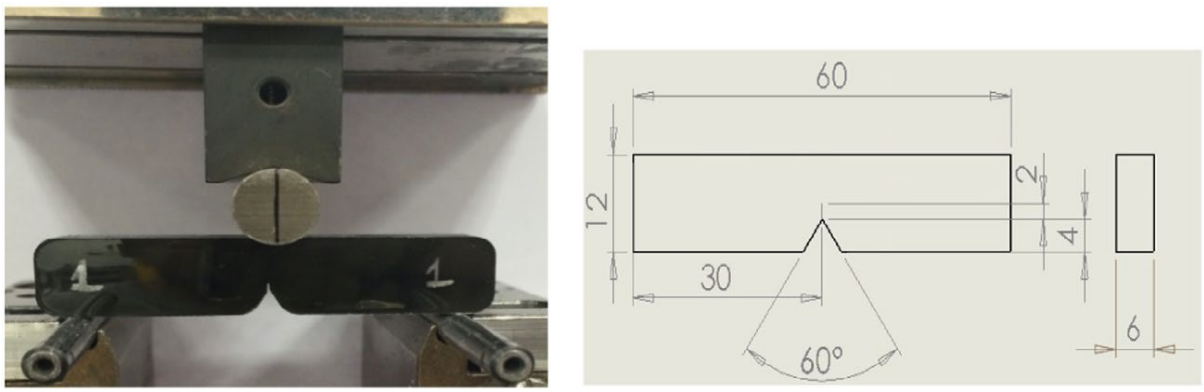

Figure 2 Three-point-bend test on single-edge-notch specimen. Dimensions are in millimetres

2.6 Dynamic mechanical analysis

A Q800 Dynamic Mechanical Analysis (DMA) was used to determine the *Tg* of the nanocomposites. The measurement point for *Tg* was taken from the peak of the tan δ curve.

Table 1. Definition and units for symbols in Equations (1–3)

Parameter		Units
K_{IC}	Critical stress intensity factor	MPa $m^{1/2}$
G_{IC}	Critical strain energy release rate (mode I)	J m^{-2}
F	Force applied	N
L	Span length	mm
B	Breath of specimen	mm
W	Width of specimen	mm
a	Crack length	mm
E	Young's modulus	GPa
v	Poisson's ratio	–

Rectangular specimens of dimensions 4 x 10 x 17.3 mm were clamped using a single cantilever clamp configuration with a torque of 1 N m. The measurements were undertaken in flexure at a fixed frequency of 1 Hz and a heating rate of 3 °C per minute. The temperature range used was from 40 to 200 °C. Three specimens were tested at each nanofiller loading content.

2.7 Thermo-Mechanical Analysis (TMA)

Thermo-Mechanical Analysis (TMA) was performed using a TA Instrument Q400 to measure the dimensional changes in the nanocomposites as a function of temperature to obtain the CTE. A linear variable differential transformer (LVDT) was applied to each sample to detect any deformation due to expansion and contraction when subjected to a temperature profile. Measurements were carried out over the temperature range 40 – 180 °C at a heating rate of 3 °C per minute. Three specimens were tested at each nanofiller loading content.

3. RESULTS AND DISCUSSION

3.1 Characterization of f-GNPs

In order to evaluate the impact of f-GNP nanofillers on the mechanical properties of GNP-epoxy nanocomposites, a number of characterization techniques were used to initially assess the physical and chemical properties of the f-GNP material. SEM images show the as-received graphene nanoplatelet material (Figure 4). The layered structure of the nanoplatelets may be seen from the higher magnification inset image in Figure 4(a). The average lateral dimensions were determined to be between 1 and 3 μm. X-ray diffraction (XRD) analysis of the f-GNPs was performed in order to assess the 2-D crystallinity and interlayer spacing of the nanomaterials. The XRD pattern for f-GNP indicates the primary (002) peak present at ~26.70° which corresponds to an interlayer spacing of ~0.34 nm and is accompanied by the (004) peak occurring at 54.60° (Figure 4(b)). The analysis indicates a high degree of crystallinity from the profile of the peaks in the diffraction pattern as well as the absence of impurities or any significant amounts of corrugated or dislocated carbon species in the material.

Raman spectroscopy was used to assess the structural quality of the GNPs. From the Raman spectrum of the f-GNPs (Figure 4(c)), the principle G-band was evident at 1585 cm−1 due to the in-plane $E2$ g vibrational mode while the 2D peak due to second-order zone boundary phonons was present at 2725 cm^{-1}. The D-band seen at 1338 cm^{-1} required defects to become Raman active, either on the basal plane (such as functionalization or vacancies) or flake edges. The intensity ratio ID/IG = 0.16 (Figure 4(c)) implies a lateral flake size of ~570 nm, significantly smaller than seen from the SEM analysis.57 The Raman spectra therefore confirm a low level of chemical functionalization of the flakes. X-ray photoelectron spectroscopy (XPS) was performed to determine the bonding present in the sample and to elucidate the proportion of oxygen containing functional groups present in the f-GNP material. Analysis of the C1s signal for the f-GNPs indicates multiple bonding peaks which were fitted using Gaussian curves (Figure 4(d)). Sp2 C–C bonding, sp3 C–C bonding, and bonding due to hydroxyl and ketone functional groups were noticeable at signals with binding energy, 284.6, 285.0, 286.6, and 287.5 eV, respectively. By analyzing the survey scan we find a carbon-to-oxygen ratio of 24, comparable to reduced graphene oxide, according to the classification.

The characterization of the f-GNPs indicated that the material comprised a highly crystalline graphitic phase, which included the presence of oxygen containing surface functional groups. The aspect ratio of the f-GNPs used here was found to be 432, which is comparable to material used in previous studies, which ranged from 90 to 933. However it has been suggested that aspect ratios as high as 35 000 are needed for full stress transfer into the filler particles, implying that the current system will not achieve optimized reinforcement. It was also noted that the presence of functional groups on the f-GNPs may improve the interfacial stress transfer.

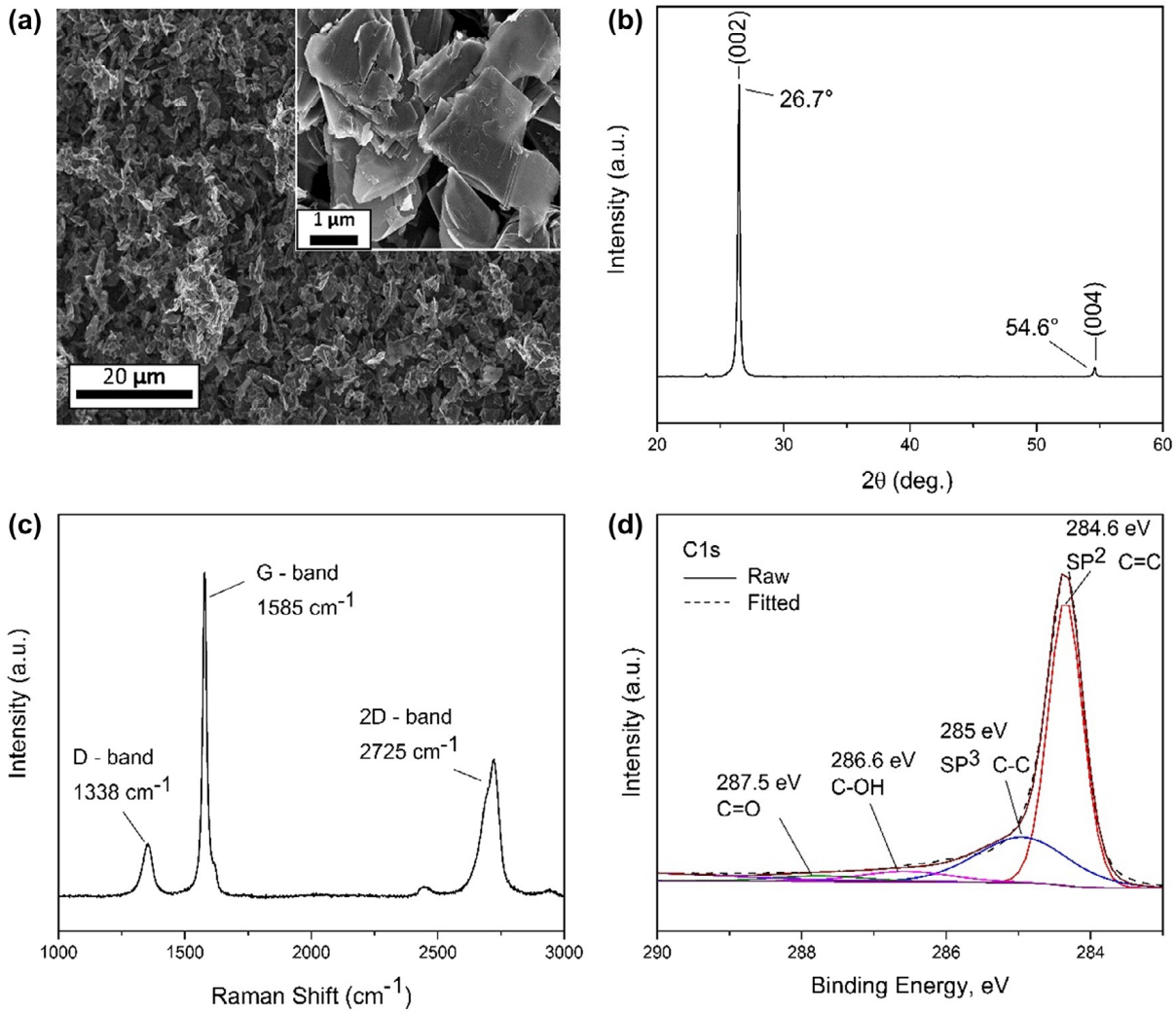

Figure 3. (a) SEM images of graphene nanoplatelets (f-GNP) with enlarged scale. (b) XRD pattern for f-GNP showing an interlayer d-spacing of ~0.34 nm at (002) peak. (c) Raman spectroscopy for f-GNP. (d) XPS C1s signal for f-GNP showing various acid groups

3.2 Tensile property

The mechanical properties (E, UTS, EL, and T) obtained from tensile tests for the neat epoxy and for the nanocomposite after the introduction of f-GNP nanofiller are analyzed. A series of f-GNP loading contents up to 1.0 wt. % were prepared using the normal cure ratio. Figure 6 shows the results of Young's modulus (E), ultimate tensile strength (UTS), elongation at break (EL), and toughness (T) of the f-GNP/epoxy nanocomposites as a function of filler content. The values plotted are the means of the six specimens tested, and the error bars show the standard deviation calculated for each loading content. Based on these plots, it can be seen that all the parameters studied showed slight enhancement with the inclusion of f-GNP nanofiller. The average values and increase over the pure epoxy matrix are also shown in Table 2.

The Young's modulus for the neat epoxy recorded a value of 2.49 GPa, which showed little significant change with increased f-GNP loading, with the standard deviation of the measured values overlapping across the full loading range. We have fitted the experimental data (up to 0.25 wt. %) to a Halpin-Tsai model in order to assess the quality of stress transfer from the matrix to the flakes. We find a predicted stiffness of the f-GNP flakes of 171 ± 7 GPa, which is significantly lower than the value of 1 TPa predicted and measured for isolated monolayer grapheme. As a result of the weak bonding between layers, it has been shown that multilayer flakes have a lower effective modulus than monolayer. For 6 layer flakes, this has been calculated to be around 550 GPa, which is still significantly higher than our calculated value. This suggests that we have very poor stress transfer, and far from optimized reinforcement from the flakes. This is likely to be a result of the relatively small lateral size of the flakes, and while the functionalization on the surface of the flakes has improved dispersability, it has not significantly enhanced the interaction with the matrix. It could also indicate the presence of voids, developed due to viscosity build-up with increasing nanofiller loading contents. Increasing the loading of the nanofiller would necessitate a meticulous approach into the processing of the nanocomposites due to the dissimilar behaviour of cross-linking and curing among other critical factors.

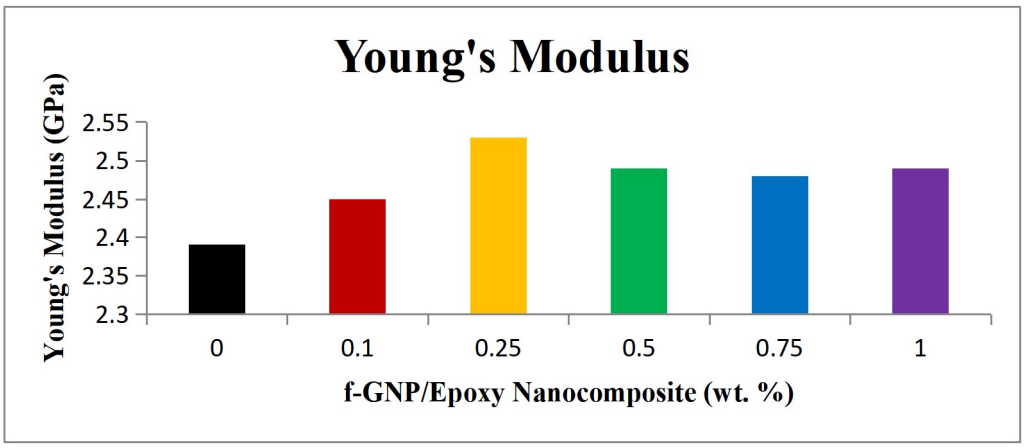

(a)

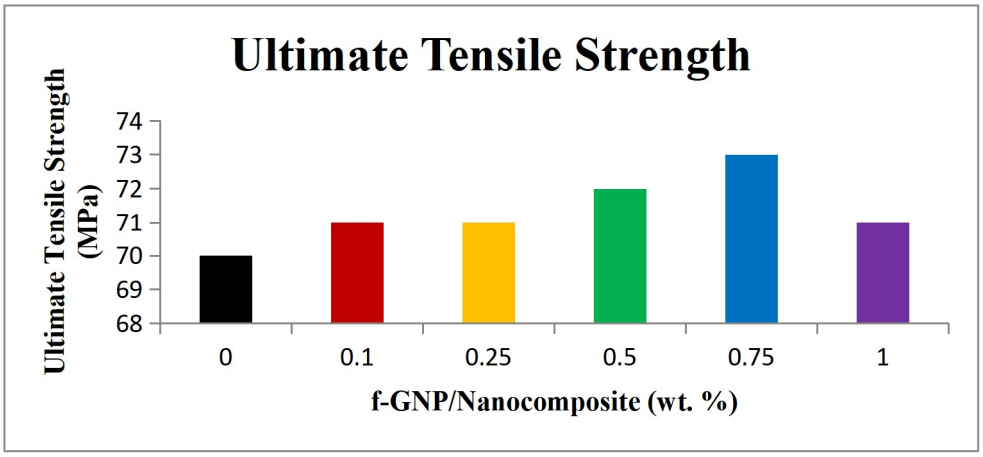

(b)

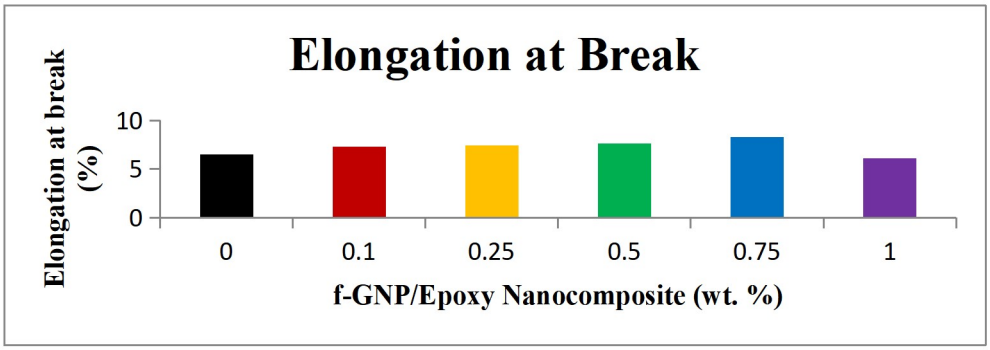

(c)

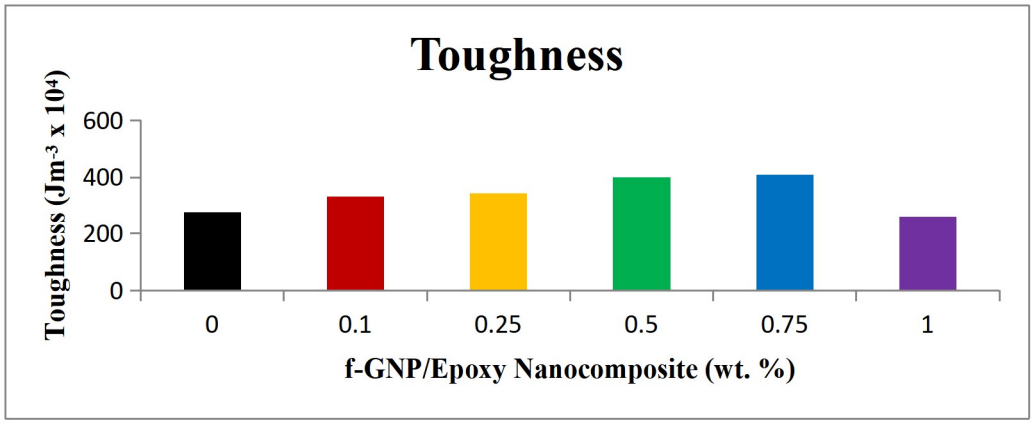

(d)

Figure 4 (a) Young's modulus, (b) Ultimate tensile strength (UTS), (c) Elongation at break (%), (d) Toughness from stress–strain curve of neat epoxy and f-GNP /Epoxy nanocomposites. In all cases, error bars indicate standard deviation

While the stiffness of the composites showed a slight increase with low loadings of f-GNPs, there was effectively no change in the UTS values measured. A very small increase in the mean values was seen up to 0.75 wt. %, although these increases are within the standard deviation of the measurements. Beyond this point, at 1 wt. % loading, the value of the UTS dropped to 72 ± 3 MPa, 1.5 % higher than the neat epoxy, although again, it is difficult to assign significance to this drop.

More significant improvements were seen in the measured values of elongation at break and in toughness. For both properties, maximum values were obtained at 0.75 wt. %, showing increases of 23.7 % and 36.3 %, respectively, over the neat epoxy. While the standard deviations in these measurements are still large, there is clear improvement over the pure epoxy at 0.75 wt. % loading of f-GNPs. A clear decrease in both properties occurred at 1.0 wt. %, a drop by 5.3 %, and 4.0 % in EL and T, respectively. Such decreases at high loading content are often observed and associated to the agglomeration of the nanomaterials1, suggesting the mixing process used here is not optimized for high loadings.

3.3 Fracture toughness

The mode I fracture toughness results measured by single edge- notch 3-point bending (SENB) tests are summarized in Figure 7 and Table 3. G_{IC} increases with increasing f-GNP loadings up to 0.25 wt. %. An increase of 51.2 % for G_{IC} was attained at this particular loading with respect to the control system, reaching a value of 245 ± 31 $J\,m^{-2}$, the highest value obtained in this series. A further increase in concentration up to 1.0 wt% led to a decline in the fracture toughness properties. This reduction in fracture toughness enhancement could be associated to the ineffective cross-linking and less effective dispersion of f-GNP at higher loading contents. This occurrence has been observed by several researchers where an increase in the loading content resulted in the weakening of the mechanical properties of nanocomposites.

SEM analysis of the fracture surfaces has been carried out to investigate the toughening mechanism of operating in our samples (Figure 6). Overall, the samples reinforced with f-GNPs show a rougher fracture surface than pure epoxy, as expected from increased toughness samples. The toughening mechanisms in the reinforced epoxy matrices can be categorized as on-plane processes (crack pinning, crack deflection immobilized layer of polymer) or off-plane processes (debonding) as highlighted. Fracture surfaces of the unmodified epoxy (Figure 6(a) and (b)) show feather markings, which is indicative of crack forking in brittle failure.

In contrast, the fracture surfaces of 0.25 wt. % f-GNP samples show bowing lines, suggesting crack pinning is occurring. For effective crack-pinning to occur, the reinforcing particles need to be larger than the crack-opening displacement.59 Using an Irwin analysis to model the plastic zone, crack-opening displacement can be calculated. The maximum value in this work is found to be 3.4 μm for 0.25 wt% f-GNP loading.

Table 2.Variation of E, UTS, %EL, and T for different f-GNP loadings relative to the neat epoxy

Loading wt%	E (GPa)	Increase (%)	UTS (MPa)	Increase (%)	EL (%)	Increase (%)	T ($\vec{J}\,m^{-3} \times 10^4$)	Increase (%)
0	2.39	N/A	70	N/A	6.5	N/A	274	N/A
0.1	2.45	+2.5	71	+1.4	7.3	+12.3	332	+21.2
0.25	2.53	+5.9	71	+1.4	7.4	+13.9	344	+25.6
0.5	2.49	+4.2	72	+2.9	7.6	+16.9	401	+46.4
0.75	2.48	+3.8	73	+4.3	8.3	+27.7	410	+49.6
1.0	2.49	+4.2	71	+1.4	6.1	-6.2	259	-5.5

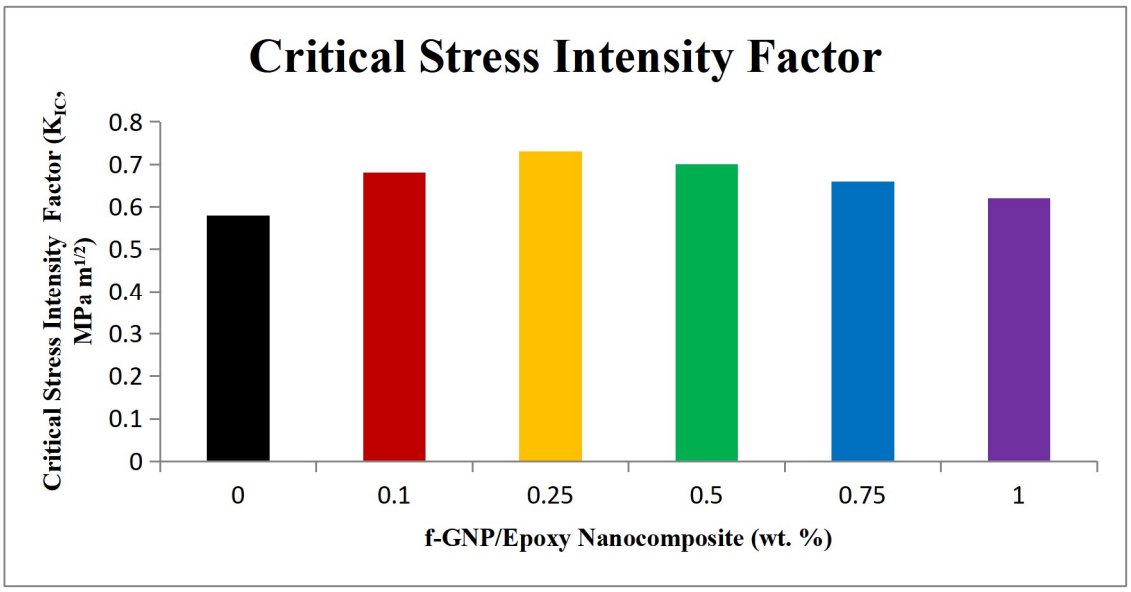

(a)

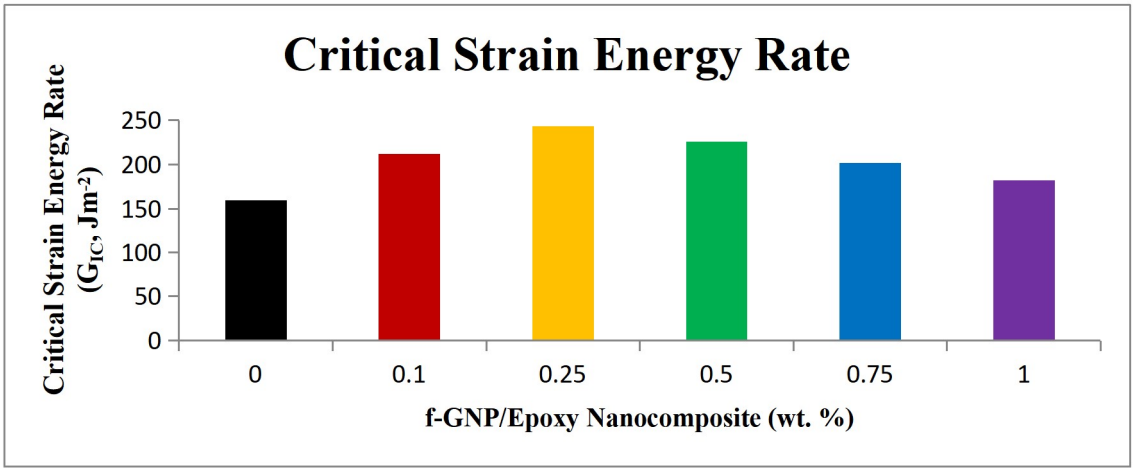

(b)

Figure 5 (a) Critical stress intensity factor, K_{IC} and (b) Critical strain energy rate, G_{IC} for f-GNP/Epoxy nanocomposites for different nanofiller loadings. In all cases, error bars indicate standard deviation

Although this is close to the lateral size of the f-GNPs used in this study, it suggests that crack-pinning is likely to be contributing to the toughening. It has been observed that the formation of an immobilized polymer layer around nanoparticles can contribute to the toughening of nanocomposites.

Table 3 Variation of K_{IC} and G_{IC} for different f-GNP loadings relative to the neat epoxy

Loading (wt%)	K_{IC} (MPa m$^{1/2}$)	Increase (%)	G_{IC} (J m^{-2})	Increase (%)
0	0.58	N/A	160	N/A
0.1	0.68	+17.2	212	+32.5
0.25	0.73	+25.9	243	+51.9
0.5	0.70	+20.7	226	+41.3
0.75	0.66	+13.8	202	+26.3
1.0	0.62	+6.9	182	+13.8

However, our measurements of glass transition temperature (see below) indicate that this is not a significant factor in our system.

Upon further examinations at higher magnifications, the 0.25 wt. % and 0.75 wt. % samples both revealed the presence of voids as well as evidence of several micro-cracks. Figure 6(c) and (d) for the specimen with 0.25 wt. % loading also indicates the presence of trenches which signifies high degree of deformation. The f-GNP operates as a stress concentrators which thereby causes several micro-cracks. At 0.75 wt. %, clusters as well as cracks were found as shown in Figure 6(e), with voids as indicated by the red arrows in Figure 6(f).

3.4 Evaluation of thermal properties

Thermal analysis using DMA was conducted to study the interaction between the nanofiller and the matrix. This technique can be used to measure the T_g, the temperature at which the material transitions from the glassy to rubbery state, and which is a fundamental property of polymers.

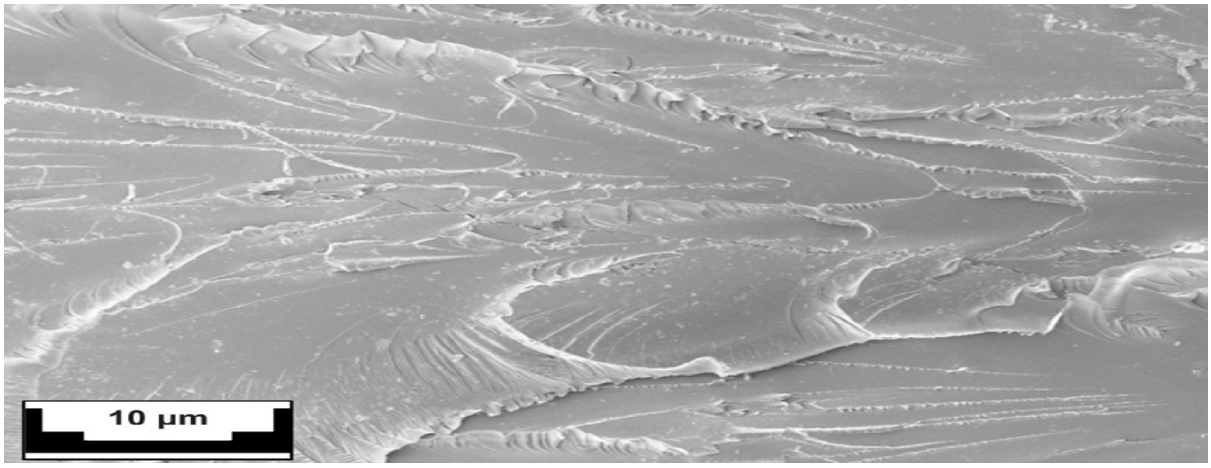

Figure 6(a). SEM Micrographs of the fracture surface for neat epoxy at magnification (500×)

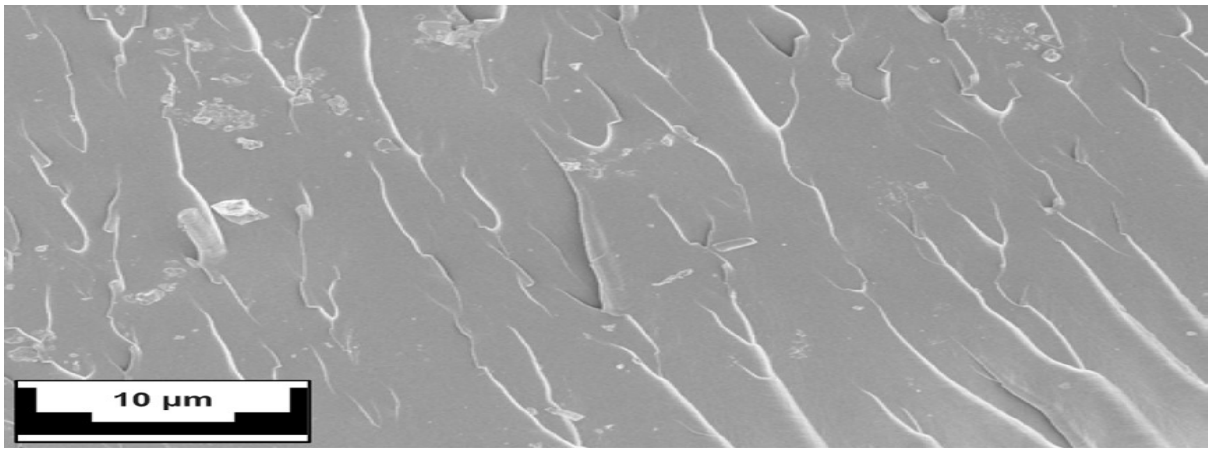

Figure 6(b). SEM Micrographs of the fracture surface for neat epoxy at magnification (5000×)

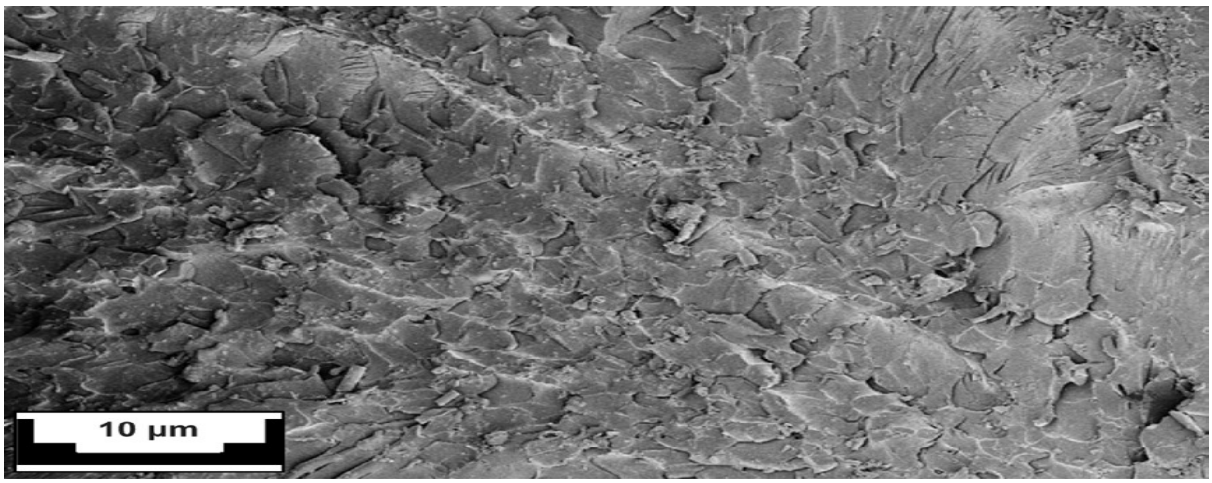

Figure 6(c). SEM Micrographs of the fracture surface for 0.25 wt% f-GNP/Epoxy at magnification (500×)

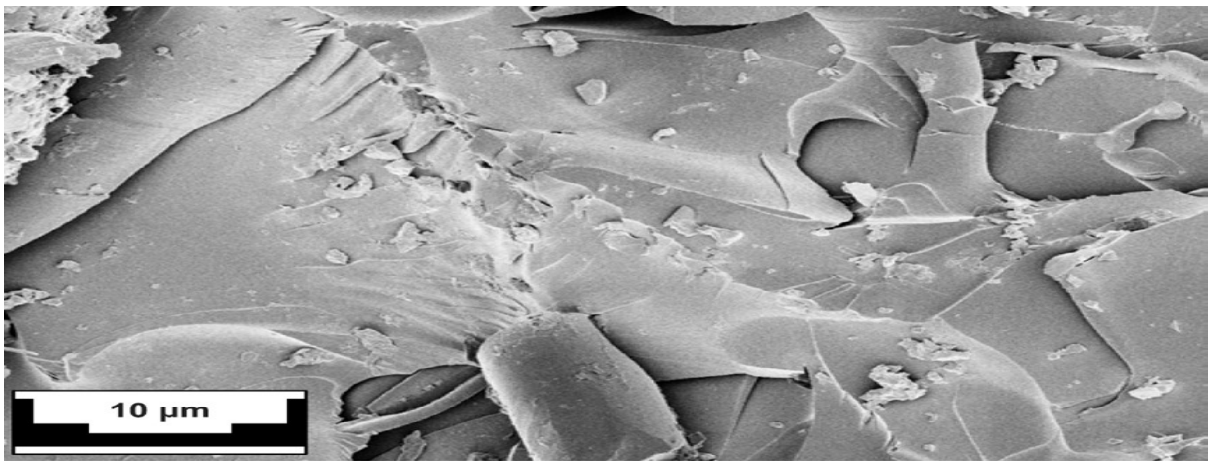

Figure 6(d). SEM Micrographs of the fracture surface for 0.25 wt% f-GNP/Epoxy at magnification (5000×)

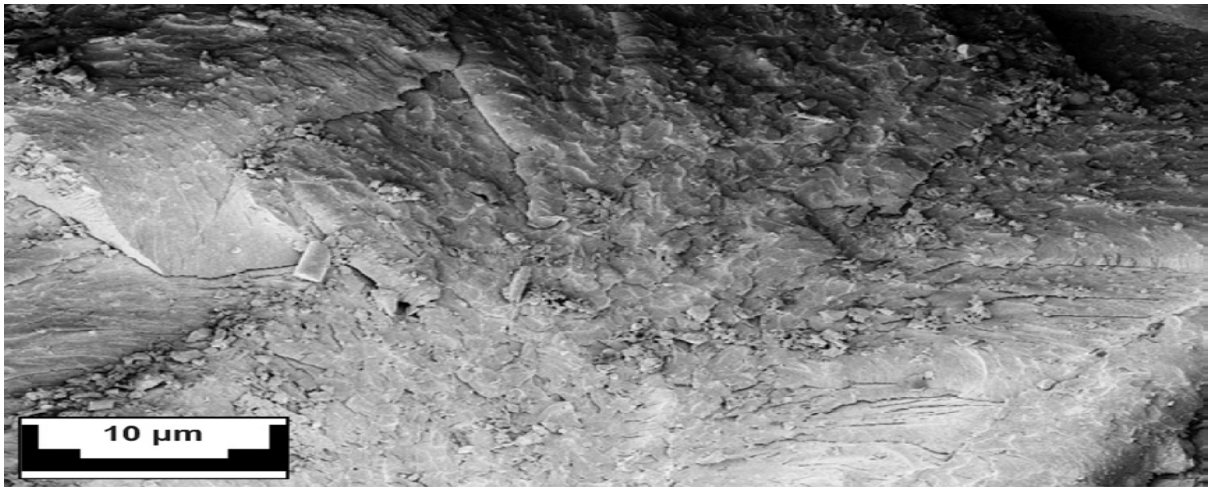

Figure 6(e). SEM Micrographs of the fracture surface for 0.75 wt% f-GNP/Epoxy at magnification (500×)

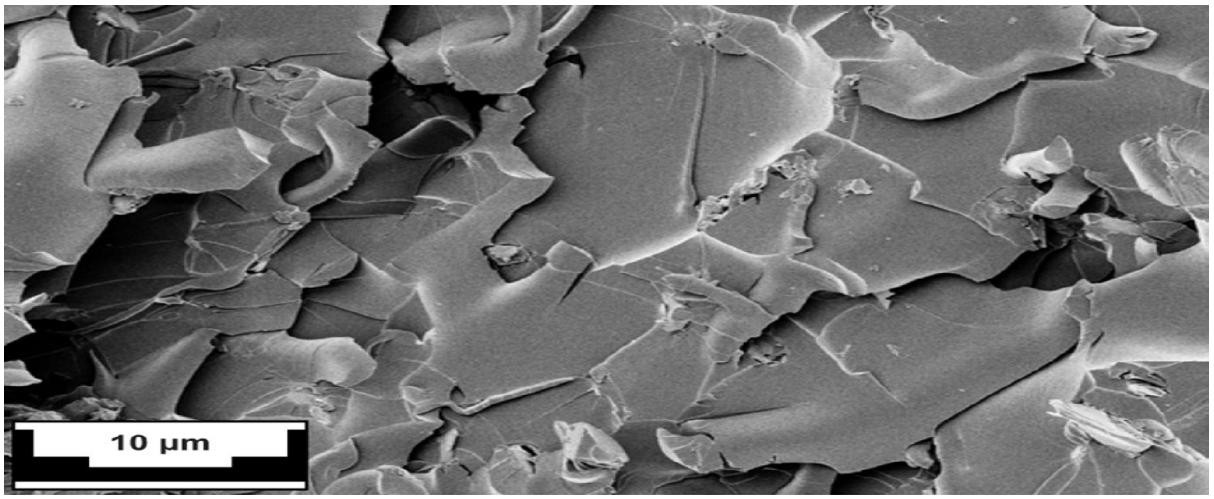

Figure 6(f). SEM Micrographs of the fracture surface for 0.75 wt% f-GNP/Epoxy at magnification (5000×)

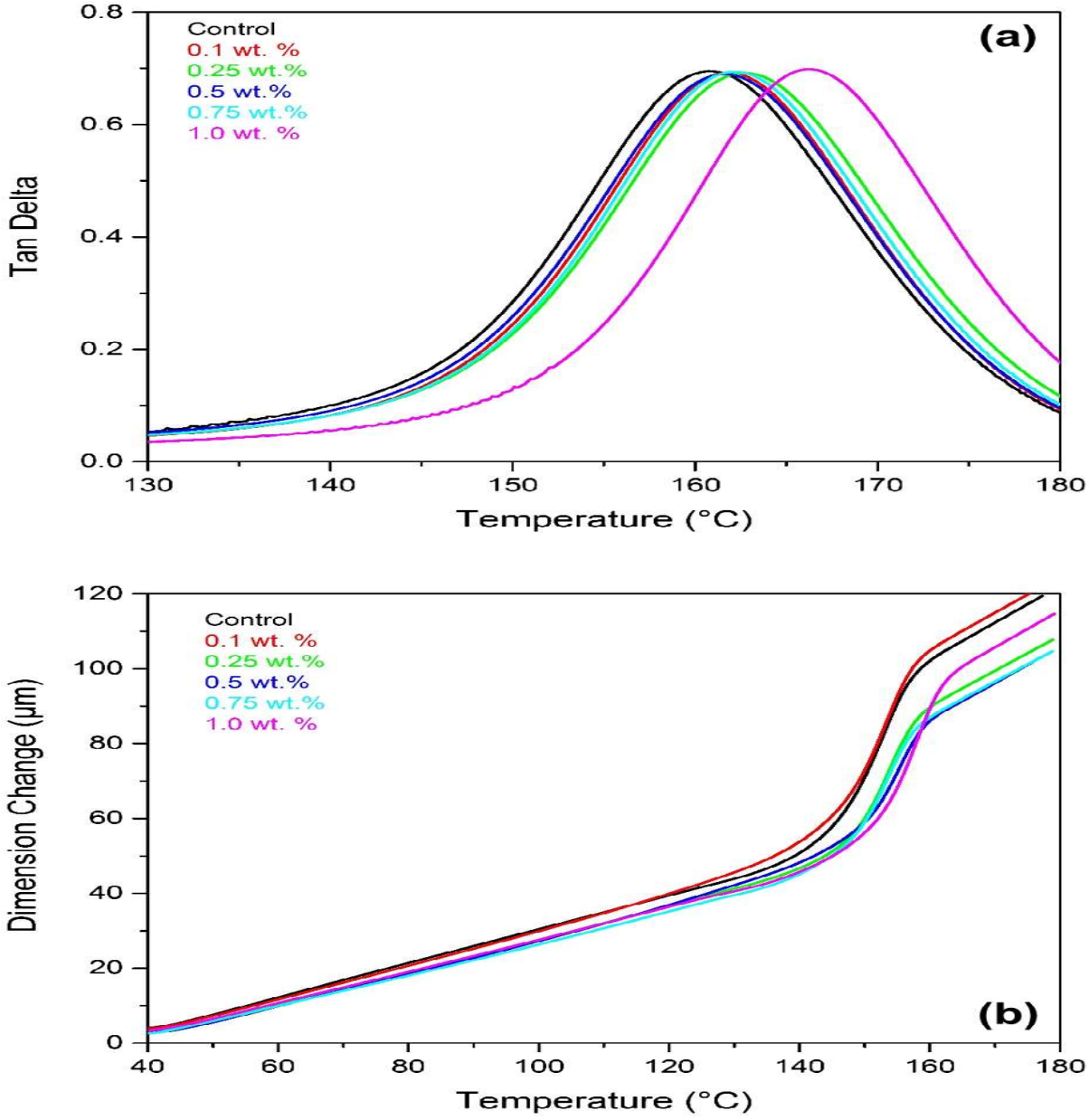

Figure 7. Damping behavior (a) tan δ and (b) TMA curve of pristine epoxy and f-GNP/Epoxy at various loadings

Table 4 Glass transition temperature *Tg* and CTE of the nanocomposites

Loading (wt%)	*Tg* by DMA (°C)	CTE by TMA ($\times 10^{-6}$ K^{-1})
0	161 ± 0.3	85 ± 0.3
0.1	162 ± 0.5	89 ± 1.1
0.25	164 ± 0.6	87 ± 1.2
0.5	162 ± 0.7	88 ± 1.6
0.75	163 ± 0.5	86 ± 1.4
1.0	166 ± 0.8	83 ± 0.9

A higher *Tg* therefore increases the allowable operating temperature of the polymer. Several aspects influence the nanocomposite's T_g, including the polymer structure, degree of cure, structural rigidity, and changes in molecular weight due to addition of the nanofiller. Curves of tan δ as a function of temperature for samples at different f-GNP loadings as well as the control system (neat epoxy) are plotted in Figure 9(a).

The T_g value derived from the tan δ curves (Figure 7(a) and Table 4) showed a value of 161 °C for the neat epoxy. A T_g value of 162 °C and 164 °C, can be observed at 0.1 wt% and 0.25 wt. %, respectively. The highest value achieved

was at 1.0 wt%, an increase of 3.2% over the pure epoxy. The increment in T_g with the incorporation of nanofiller is a result of the strong interface between the latter and the epoxy molecules, the restriction in the vibration of chain molecules and effective cross-linking mechanisms which demonstrate fundamental alteration in polymer chain dynamics.

The CTE was determined for the neat epoxy and the nanocomposites. The CTE is calculated by measuring the variation in the length of the component under heating or cooling. Attaining a low CTE and excellent thermal stability are criteria that need to be achieved when there is a change in temperature in different engineering applications. CTE values can be reported between two parts of the TMA curve, below (60 –120 °C) or above the T_g (160 –175 °C). The

CTE reported in this study was below $T_g$as polymers or nanocomposites suffer a drop in their mechanical properties above T_g. As shown in Table 4, the neat epoxy recorded a value of 85 . $10^{-6}\ K^{-1}$. CTE values increased at 0.1 wt% before decreasing to a value of 86. $10^{-6}\ K^{-1}$at 0.75 wt. %. Promising results were achieved at 1.0 wt. % where a value of 83. $10^{-6}\ K^{-1}$, a decrease of 2.1 % relative to the neat epoxy.

The beneficial impact of using commercial grapheme nanoplatelets demonstrated in this work may be readily translated toward bulk scale manufacturing and it can be achieved at low cost. This is directly relevant to the aerospace and automotive sectors among others. In Table 5 we compare our toughening results to previous studies on epoxy resins reinforced with various nanofillers. It can be seen that the best result from the current work (51% improvement at 0.25 wt. % filler content) is among the best reported in the literature. While comparable toughening has been achieved using clay reinforcement this was at a filler content four times higher than we have used. Similarly, the best reported values for GNPs (46 % improvement) was found for 1.0 wt. % filler content. 48 Although the use of silica nanoparticles has shown improvements in fracture toughness of over 270 %, this was seen at filler contents of 20 wt. %, two orders of magnitude high than our best results.

In this work, we observed encouraging fracture toughness properties at a much lower loading content using f-GNP as nanofiller. The intrinsically small nature of unfunctionalized GNPs generally causes agglomeration. However, the GNPs used in this study were functionalized via plasma which enabled greater dispersibility and exfoliation of the grapheme nanoplatelets. A substantial increase by over 50% with the incorporation of 0.25 wt% f-GNP loading has been achieved. This had no detrimental effect on the tensile and thermal properties of the nanocomposites.

4. CONCLUSION

A series of plasma functionalized graphene nanoplatelet (f-GNP) based epoxy nanocomposites were fabricated in an attempt to study the effect of f-GNP on the mechanical and thermal properties of the epoxy. The processing of the nanocomposites was carried out by solvent-assisted techniques using methanol. The variations in tensile strength, Young's modulus, elongation at break, and fracture toughness properties were studied as well as the morphology of the fracture surface. It was observed that maximum UTS occurred at 0.75 wt. % of f-GNP with a value of 74 MPa, an increase of 4.9 % compared with the neat epoxy. The maximum stiffness was achieved at 0.25 wt. %, 5.6 % higher than in the pure epoxy, whereas the highest value obtained for elongation at break was at 0.75 wt. %, a value of 9.3 % in comparison with 7.5 %. Optimal mode I fracture toughness performance, G_{IC}, was noticed at 0.25 wt. %, an impressive improvement of 51.2 % higher than the neat epoxy. This was attributed to the preparation of homogenous dispersions of GNP in the nanocomposite which were obtained using a solvent extraction processing technique, thereby increasing the performance significantly due to load transfer of the nanomaterials. Evidence from fractography analysis showed crack pinning and crack deflection including micro cracks. Evidence was also seen of voids which were attributed to the plastic void growth. The use of plasma functionalization on graphene nanoplatelets implies that no acid treatment was involved during functionalization, allowing an environmentally friendly and cost-effective solution for the preparation of scalable epoxy nanocomposites. Glass transition temperature, T_g derived from DMA, and CTE derived from TMA both exhibited an increase at 1.0 wt. %, an increment of 3.2 % and 2.1 %, respectively, in comparison with the neat epoxy. By comparing our results to reported improvements in fracture toughness, we have shown that we have exceeded the best previous results, but at significantly lower filler contents. Reducing the amount of (relatively) expensive filler component is important for commercial use of these nanocomposite materials. This work demonstrates a robust strategy for the preparation of f-GNP/epoxy nanocomposites which exhibit enhanced mechanical properties. The findings presented here also provide a basis for further studies to investigate toughening mechanisms under further optimized processing conditions.

Conflict of interest

The authors declare that there is no conflicting interest in the publication of this paper.

Acknowledgements
This paper was not supported by any financial grant from granting bodies. The authors really appreciate by acknowledging Engr.Dr.George O.O. for his active inputs and contributions needed for the outcome of this publication financially and otherwise.

References

Boland, C. S., Barwich, S., Khan, U., and J. N. Coleman, J. N. (2016). 'High stiffness nanocomposite fibres from polyvinylalcohol filled with graphene and boron nitride', *Carbon*, 99, 280–288.

Kausar, A., Anwar, Z., and B. Muhammad, B. (2016). 'Recent developments in epoxy/graphite, epoxy/graphene, and epoxy/graphene nanoplatelet composites: a comparative review', *Polym. Plast. Technol. Eng.*, 55, 1192–1210.

Sainsbury, T., Gnaniah, S., Spencer, S. J., Mignuzzi, S., Belsey, N. A., Paton, K. R., Satti, A. (2016). 'Extreme mechanical reinforcement in grapheme oxide based thin-film nanocomposites via covalently tailored nanofiller matrix compatibilization', *Carbon*, 2016, 114, 367–376.

Stevens, B., Guin, T., Sarwar, O., John, A., Paton, K. R., Coleman, J. N., Grunlan, J. C. (2016). 'Highly conductive graphene and polyelectrolyte multilayer thin films produced from aqueous suspension', *Macromol. Rapid Commun.*, 37, 1790–1794.

Tabandeh-Khorshid, M., Omrani, E., Menezes, P. L., Rohatgi, P. K. (2016). 'Tribological performance of self-lubricating aluminium matrix nanocomposites: role of graphene nanoplatelets', *Eng. Sci. Technol. Int. J.*, 2016, 19, 463–469.

Boland, C. S., Khan, U., Ryan, G., Barwich, S., Charifou, R., Harvey, A., Backes, C., Z. Li, Z., Ferreira, M. S., Mobius, M. E., Young, R. J., Coleman, J. N. (2016). 'Sensitive electromechanical sensors using viscoelastic graphenepolymer nanocomposites', *Science*, 354, 1257–1260.

Liu, Y., Wu, H., Chen, G. (2016). 'Enhanced mechanical properties of nanocomposites at low graphene content based on *in situ* ball milling', *Polym. Compos.*, **37**, 1190–1197.

Dornbusch, M., Christ, U., Rasing, R. (2016). 'Epoxy resins: fundamentals and applications. Reactive Polymers Fundamentals and Applications', Vicenta Network.

Kemp, M. (2016). 'Unlocking the potential of graphenes for the development of multi-scale composites – functionalization via plasma', *Reinf. Plastic.*, 60, 332–334.

Backes, C., Paton, K. R., Hanlon, D., Yuan, S., Katsnelson, M. I., Houston, J., Smith, R. J., McCloskey, D., Donegan, J.F., Coleman, J. N. (2016). 'Spectroscopic metrics allow *in situ* measurement of mean size and thickness of liquid-exfoliated few-layer graphene nanosheets', *Nanoscale*, 8, 4311–4323.

King, A. A., Davies, B. R., Noorbehesht, N., Newman, P., Church, T. L., Harris, A. T., Razal, J. M., Minett, A. I. (2016). 'A new Raman metric for the characterisation of graphene oxide and its derivatives', *Sci. Rep.*, 6, 2824.

Li, Y., Zhang, H., Porwal, H., Huang, Z., Bilotto, E., Peijs, T. (2017). 'Mechanical, electrical and thermal properties of *in situ* exfoliated graphene/epoxy nanocomposites', *Compos. Part A Appl. Sci. Manuf.*, 95, 229–236.

Mushtaq, A., Mukhtar H. B., Shariff, M. A .(2016). 'Effect of glass transition temperature in enhanced polymeric blend membranes', *Procedia Eng.*, 148, 11–17.

Zagho, M. M., Hussein, E. A., and Elzatahry, A. A. (2018). "Recent overviews in functional polymer composites for biomedical applications," *Polymers*, vol. 10, no. 7, p. 739, doi: 10.3390/polym10070739.

Darshan S. M., and Suresha, B. (2021). "Effect of basalt fiber hybridization on mechanical properties of silk fiber reinforced epoxy composites," *Materials Today: Proceedings*, vol. 43, pp. 986–994, doi: 10.1016/j.matpr.2020.07.618.

Darshan, S. M., Suresha, B., and Jamadar, I. M. (2022). "Optimization of Abrasive Wear Parameters of Halloysite Nanotubes Reinforced Silk/Basalt Hybrid Epoxy Composites using Taguchi Approach," *Tribology in Industry*, vol. 44, no. 1, pp. 253–267, doi: 10.24874/ti.1131.06.21.08.

Darshan S. M., and Suresha, B. (2022). "Effect of halloysite nanotubes on Physico-Mechanical Properties of Silk/Basalt fabric reinforced epoxy composites," *Materials Science Forum*, vol. 1048, pp. 21–32, doi: 10.4028/www.scientific.net/msf.1048.21.

Namdev, A., Telang, A., and Purohit, R. (2022). "Experimental investigation on mechanical and wear properties of GNP/Carbon fiber/epoxy hybrid composites," *Materials Research Express*, vol. 9, no. 2, p. 025303, doi: 10.1088/2053-1591/ac4e3f.

Vinod, Kumar, A., Suresha, B., Kumar, M., and Ramesh, S. (2018). "Study on Two Body Abrasive Wear behaviour of Carboxyl-Graphene Reinforced Epoxy Nano-composites," *IOP Conference Series: Materials Science and Engineering*, vol. 376, p. 012058, doi: 10.1088/1757-899x/376/1/012058.

Namdev, A., Purohit, R., and A. Telang, A. (2023). "Impact of graphene nano particles on tribological behaviour of carbon fibre reinforced composites," *Advances in Materials and Processing Technologies*, pp. 1–18, doi: 10.1080/2374068x.2023.2189670.

Namdev, A., Telang, A., Purohit, R., and M.K. Agrawal, M. K. (2022). "An experimental assessment of abrasive wear behavior of GNP/Carbon fiber/epoxy hybrid composites," Indian Journal of Engineering and Materials Sciences, vol. 29, no. 6, pp. 777–785, doi: 10.56042/ijems.v29i6.70309.

Kumar, S., Singh, K. K., and Ramkumar, J. (2020). "The effects of graphene nanoplatelets on the tribological performance of glass fiber-reinforced epoxy composites," *Proceedings of the Institution of Mechanical Engineers, Part J: Journal of Engineering Tribology*, vol. 235, no. 8, pp. 1514–1525, doi: 10.1177/1350650120965756.